

Exciton in Semiconductor Quantum Box: An Important Analytical Computational Step

A. EL HADDAD*

*Regional Center for Education and Training Professions, Department of Physical Sciences,
Avenue My Abdelaziz Souani 90100, Tangier, Morocco*

Received: 14.11.2022 & Accepted: 28.12.2022

Doi: [10.12693/APhysPolA.143.246](https://doi.org/10.12693/APhysPolA.143.246)

*e-mail: a_haddad01@yahoo.fr

A theoretical model to determine the properties of an exciton confined in a semiconductor quantum box with rectangular potential is presented. We have used the two-band model and the effective mass approximation. The theoretical approach includes a considerable analytic phase and makes it possible to reduce the numerical calculations. According to the new formulation, the limit cases for an exciton in a bulk semiconductor and an exciton confined in a two-dimensional structure are deduced, and a good agreement is shown in comparison with known results in the literature. We calculated the binding energy, spatial extension, and effective Bohr radius of the exciton. The variation law of the confined exciton energy, as a function of the dimension of the semiconductor quantum box, is established. The illustrations are given for a rectangular confining potential with finite and infinite barriers.

topics: exciton, analytical formulation, binding energy, effective Bohr radius

1. Introduction

The rapid progress of nanometer-scale fabrication technologies in recent years has enabled the construction of low-dimensional semiconductor nanostructures. These systems have become the object of extensive research activity due to their promising technological applications. They will form the basis of the electronic and optical devices of the future. The optical properties of these structures are dominated by excitonic effects. An exciton is a quasi-particle that consists of an electron-hole pair bonded by the Coulomb interaction. Excitonic effects are important in the development of stable and high-efficiency nanoscale optoelectronic devices. Through the localization of charge carriers, excitonic effects are enhanced in low-dimensional nanostructures compared to bulk semiconductors.

In the last decades, several studies have focused on excitonic states in semiconductor nanostructures. In the particular case of excitons confined in three directions of space, also called the zero-dimensional (0D) nanostructure, the models used are quite diverse. This diversity concerns both the geometric shape of the structure and the profile of the associated confinement potential. There have been several reports on excitonic phenomena in 0D nanostructures where they are described as rectangular quantum boxes (QB) with a finite or infinite confinement barrier [1–3], spherical quantum dots with a rectangular potential barrier [4, 5], parabolic [6–8] and gradual potential profile [9]. We

found also a description of 0D nanostructures as cylindrical [10–16], conical [17], triangular [18], and lens-shaped quantum dots [19].

Exciton states confined in nanostructures have often been investigated theoretically by using either the variational approach [1, 2, 20] or the configuration-interaction approach [3, 21]. In the variational approach, the exciton wave function is represented by a trial function. However, in the configuration-interaction approach, the exciton wave function is expanded in terms of an appropriate basis set, and thus the ground and excited states can be described accurately with a large number of bases. It was reported by Kubota and Nobusada [3] that the validity of the variational approach depends on the choice of the trial function and, in general, its application to excited excitonic states is practically difficult, but the configuration-interaction approach requires huge computational costs. Planelles and Climente [22] have calculated the ground state energy of neutral and charged excitons confined in semiconductor quantum dots by using the variational Quantum Monte Carlo method.

So, the calculations of excitonic states presented in the literature are essentially based on numerical methods and require heavy calculations with powerful machines. Thus, it would be interesting to provide a simple, fast, accurate, and useful analytical formulation that can be easily applied to determine the exciton properties in 0D semiconductor nanostructures.

In this work, we present a method that uses a rather important phase of analytical calculation, considering the 0D nanostructure as a rectangular quantum box (QB). This makes it possible to greatly limit the use of numerical calculations and to find the desired results in a short time. In order to calculate the binding energy, spatial extension, and effective Bohr radius of an exciton in a quantum box, we develop a calculation model, which includes a considerable analytical phase and is valid for any shape of the confining potential, provided that the solution of the one-particle problem is known. The formulation is performed in the framework of the effective mass approximation and the two-band model.

The paper is organized as follows. In the next section, we formulate the assumptions and equations of the model. Expressions of the binding energy, spatial extension, and effective Bohr radius of the exciton are presented. Two-dimensional (2D) and three-dimensional (3D) limit cases are deduced. The application of the calculation model for rectangular QB is discussed in Sect. 3. A brief summary is presented in the last section.

2. Model calculation

2.1. Basic equations

We consider a single quantum box of type I of dimensions L_x , L_y , and L_z along the x -, y -, and z -axis, respectively. The confining potential is of arbitrary shape, say $V_e(x_e, y_e, z_e)$ for an electron and $V_h(x_h, y_h, z_h)$ for a hole. Throughout the paper, we use effective atomic units, which means that all distances are measured in units of the exciton Bohr radius $a_B = \hbar^2 \varepsilon / (\mu^* e^2)$, energies in units of the Rydberg constant $Ry = \mu^* e^4 / (2\hbar^2 \varepsilon^2)$, masses in units of the reduced electron-hole mass μ^* , where $\frac{1}{\mu^*} = \frac{1}{m_e^*} + \frac{1}{m_h^*}$, and $m_{e(h)}^*$ is the effective masses of electron (hole).

In the hypothesis of uncoupled excitons, the Hamiltonian operator of one exciton (X), in the effective mass approximation, is given by

$$H = H_e + H_h + H_C, \quad (1)$$

with

$$H_i = -\frac{\partial}{\partial x_i} \left(\frac{\partial}{m_i \partial x_i} \right) - \frac{\partial}{\partial y_i} \left(\frac{\partial}{m_i \partial y_i} \right) - \frac{\partial}{\partial z_i} \left(\frac{\partial}{m_i \partial z_i} \right) + V_i(x_i, y_i, z_i), \quad (2)$$

where $i = e, h$, and

$$H_C = -\frac{2}{r}. \quad (3)$$

In the above equations, H_e (H_h) describes the movement of an electron (hole) with energy E_e (E_h); H_C is the Coulomb interaction term; r is the relative position $r = \sqrt{(x_e - x_h)^2 + (y_e - y_h)^2 + (z_e - z_h)^2}$, and ε represents the dielectric constant (assumed to be equal inside and outside the box).

The exciton wave function is chosen to be of the following form

$$\Psi(\mathbf{r}_e, \mathbf{r}_h) = \Psi_e(\mathbf{r}_e) \Psi_h(\mathbf{r}_h) \Phi \quad (4)$$

where Φ is the coupling factor, which will be conveniently chosen to describe the exciton state. Thus, for the ground state X_{1s} , we take

$$\Phi = \exp\left(-\frac{r}{\lambda}\right). \quad (5)$$

The eigenstate $\Psi_i(\mathbf{r}_i)$ of one-particle Hamiltonian ($H_i \Psi_i = E_i \Psi_i$), in this work, is considered as the product of three independent functions

$$\Psi_i(\mathbf{r}_i) = f_i(x_i) g_i(y_i) h_i(z_i). \quad (6)$$

The exciton energy E_X is determined by minimizing the expectation value of H with respect to the suitable variational parameter λ . Then, the binding energy of exciton E_b is given by

$$E_b = E_e + E_h - E_X. \quad (7)$$

The effect of the mass mismatch on the binding energy is very small [23]. This effect is neglected from now on, but it is taken into account for the calculation of one-particle state. The anisotropy of the valence band is neglected.

Inserting the exciton wave function (4) into (1), we find after some algebra

$$\begin{aligned} \langle \Psi | H | \Psi \rangle &= (E_e + E_h) \langle \Psi | \Psi \rangle \\ &+ \int d\Omega \left[\frac{(\nabla_e \Phi)^2}{m_e} + \frac{(\nabla_h \Phi)^2}{m_h} - \frac{2\Phi^2}{r} \right] \Psi_e^2 \Psi_h^2 \end{aligned} \quad (8)$$

with $d\Omega = dx_e dx_h dy_e dy_h dz_e dz_h$.

The first term $\langle \Psi | \Psi \rangle$ can be written as

$$\begin{aligned} \langle \Psi | \Psi \rangle &= \int_{\mathbf{r}} d\mathbf{r} \left[\int d\mathbf{r}_e d\mathbf{r}_h |\Psi_e|^2 |\Psi_h|^2 \Phi^2 \right] \\ &\times \left(\delta(\mathbf{r}_e - \mathbf{r}_h - \mathbf{r}) + \delta(\mathbf{r}_h - \mathbf{r}_e - \mathbf{r}) \right), \end{aligned} \quad (9)$$

where $\mathbf{r} = (X, Y, Z)$ is the electron-hole relative position, which we consider with positive components. The previous expression can be transformed into the following form

$$\begin{aligned} \langle \Psi | \Psi \rangle &= \int_{\mathbf{r}} d\mathbf{r} \int d\mathbf{r}_e |\Psi_e(\mathbf{r}_e)|^2 |\Psi_h(\mathbf{r}_e - \mathbf{r})|^2 \Phi^2(\mathbf{r}_e, \mathbf{r}_e - \mathbf{r}) \\ &+ \int_{\mathbf{r}} d\mathbf{r} \int d\mathbf{r}_e |\Psi_e(\mathbf{r}_e)|^2 |\Psi_h(\mathbf{r}_e + \mathbf{r})|^2 \Phi^2(\mathbf{r}_e, \mathbf{r}_e + \mathbf{r}). \end{aligned} \quad (10)$$

We note that $\Phi(\mathbf{v}, \mathbf{v} + \mathbf{r}) = \Phi(\mathbf{v} + \mathbf{r}, \mathbf{v}) = \Phi(r)$ (see (5)). Making the substitution $\mathbf{v} = \mathbf{r}_e - \mathbf{r}$ in the first term, and $\mathbf{r}_e = \mathbf{v}$ in the second, the expression $\langle \Psi | \Psi \rangle$ can be written as

$$\langle \Psi | \Psi \rangle = \int d\mathbf{r} \Phi^2(r) P(\mathbf{r}), \quad (11)$$

where the function P is defined by

$$\begin{aligned} P(\mathbf{r}) &= \int d\mathbf{v} \left[|\Psi_e(\mathbf{v} + \mathbf{r})|^2 |\Psi_h(\mathbf{v})|^2 \right. \\ &\left. + |\Psi_e(\mathbf{v})|^2 |\Psi_h(\mathbf{v} + \mathbf{r})|^2 \right]. \end{aligned} \quad (12)$$

Owing to these transformations, the binding energy defined in (7) writes

$$E_b = -\frac{1}{\lambda^2} + \frac{2\mathcal{Y}(G)}{\mathcal{Y}(F)} \quad (13)$$

with

$$G = \frac{\Phi^2}{r} \quad (14)$$

and

$$F = \Phi^2. \quad (15)$$

The operator \mathcal{Y} is defined as

$$\mathcal{Y}(F) = \int dX dY dZ P(X, Y, Z) F(X, Y, Z), \quad (16)$$

where X, Y , and Z are the separated distance between the electron and the hole along the x -, y -, and z -direction, respectively, (e.g., $X = |x_e - x_h|$).

In the hypothesis of the one-particle eigenstate of (6), $P(X, Y, Z)$ can be written as

$$P(X, Y, Z) = P_x(X) P_y(Y) P_z(Z), \quad (17)$$

where $P_x(X)$ represents the uncorrelated probability of finding an electron and hole separated by a distance X along the x -axis [24],

$$P_x(X) = \int_{-\infty}^{+\infty} dx \left[|f_e(x+X)|^2 |f_h(x)|^2 + |f_h(x+X)|^2 |f_e(x)|^2 \right], \quad (18)$$

where f_e and f_h are the functions defined in (6).

The extension of the exciton r_{ex} , defined as $r_{ex} = \sqrt{\langle r^2 \rangle}$, is given by

$$r_{ex} = \sqrt{\frac{\mathcal{Y}(r^2 F)}{\mathcal{Y}(F)}}. \quad (19)$$

The effective Bohr radius of a quantum-confined exciton [1, 16] is defined as

$$a_{ex} = \left(\left\langle \Psi \left| \frac{1}{r} \right| \Psi \right\rangle \right)^{-1}. \quad (20)$$

The above calculation transformations make it possible to determine the binding energy, spatial extension and effective Bohr radius of the exciton, passing from integrals with six variables to integrals with three variables.

2.2. 3D and 2D limit cases

At this stage, we can deduce the behaviour of the exciton in the limiting cases 3D (bulk material) and 2D (electron and hole confined in the same plane).

In 3D limit case (L_x, L_y , and $L_z \rightarrow \infty$), the function P_x (P_y and P_z) varies slowly with X (Y and Z), and we have $\frac{\mathcal{Y}(G)}{\mathcal{Y}(F)} = \frac{1}{\lambda}$ and $\frac{\mathcal{Y}(r^2 F)}{\mathcal{Y}(F)} = 3\lambda^2$. Maximizing $E_b(\lambda)$ gives $E_b^{3D} = Ry$, with $\lambda^{3D} = a_B$. In this case, the extension of the exciton is $r_{ex} = \sqrt{3} a_B$ and its effective Bohr radius is $a_{ex} = a_B$.

In the 2D limit case corresponding to $X = 0$, (L_y and $L_z \rightarrow \infty$), we find $\frac{\mathcal{Y}(G)}{\mathcal{Y}(F)} = \frac{2}{\lambda}$ and $\frac{\mathcal{Y}(r^2 F)}{\mathcal{Y}(F)} = \frac{3\lambda^2}{2}$. Maximizing $E_b(\lambda)$ gives expressions known in the literature, i.e., $E_b^{2D} = 4Ry$ and $\lambda^{2D} = \frac{1}{2} a_B$. In this case, the extension of the exciton is $r_{ex} = \sqrt{3} a_B / \sqrt{8}$ and its effective Bohr radius is $a_{ex} = \frac{1}{4} a_B$. The r_{ex} expression above is the same as reported in [25].

2.3. Single-particle ground state

The confining potential is given by

$$V_i(x_i, y_i, z_i) = \begin{cases} 0 & \text{if } |x_i| < \frac{L_x}{2}, |y_i| < \frac{L_y}{2}, \\ & |z_i| < \frac{L_z}{2} \\ V_{0,i} & \text{otherwise} \end{cases} \quad (21)$$

$i = e, h$; L_x, L_y , and L_z are the dimensions of the box. First, we consider infinite confinement potential ($V_{0,i} = \infty$). The one-particle wave function can be written as

$$\Psi_i = \cos\left(\frac{\pi}{L_x} x_i\right) \cos\left(\frac{\pi}{L_y} y_i\right) \cos\left(\frac{\pi}{L_z} z_i\right) \quad (22)$$

In this particular case, the functions $P_x(X)$, $P_y(Y)$, and $P_z(Z)$ can be calculated analytically and take the similar form as

$$P_x(X) = (L_x - X) \left[\frac{1}{4} + \frac{1}{2} \cos^2\left(\frac{\pi X}{L_x}\right) \right] + \frac{3L_x}{4\pi} \cos\left(\frac{\pi X}{L_x}\right) \sin\left(\frac{\pi X}{L_x}\right). \quad (23)$$

For a finite barrier height $V_{0,i}$, for simplicity we considered only the square quantum box (SQB) ($L_x = L_y = L_z = L$). The ground state of the one-particle problem is solved for the x -component of the wave function by using

$$\begin{cases} f_i(x_i) = \cos(k_i x_i), & \text{if } |x_i| < \frac{L_x}{2} \\ f_i(x_i) = \cos\left(k_i \frac{L_x}{2}\right) e^{-K_i(|x_i| - \frac{L_x}{2})}, & \text{otherwise,} \end{cases} \quad (24)$$

where $K_i = \sqrt{\frac{1}{3} m_{i,b} (V_{0,i} - E)}$, $k_i = \sqrt{\frac{1}{3} m_{i,w} E}$, and

$$\frac{k_i}{m_{i,w}} \tan\left(k_i \frac{L_x}{2}\right) = \frac{K_i}{m_{i,b}}, \quad (25)$$

obtained by requiring continuity of Ψ_i (see (6)) and its partial derivatives at the interfaces, $i = e, h$; $m_{i,w}$ and $m_{i,b}$ are the effective masses inside and outside the box, respectively.

The functions $P_x(X)$, $P_y(Y)$, and $P_z(Z)$ are the same but cannot be found analytically, their values are calculated numerically (18).

3. Results and discussion

The calculations in this section have been performed assuming that the box is a GaAs well, surrounded by an $\text{Al}_{0.3}\text{Ga}_{0.7}\text{As}$ barrier. We adopted

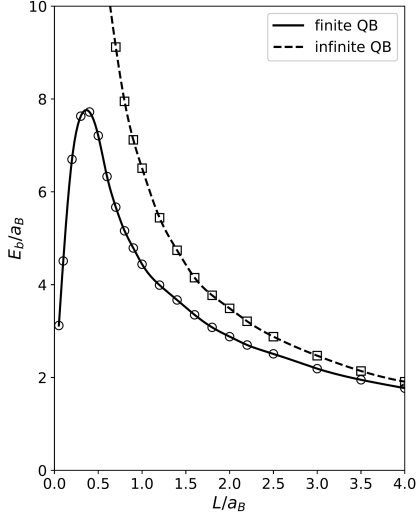


Fig. 1. Binding energy of the $1s$ confined state of a heavy-hole exciton in a GaAs quantum box with sides of length L . The results are calculated for an infinite barrier (dashed line) and a finite $\text{Al}_{0.3}\text{Ga}_{0.7}\text{As}$ barrier (solid line).

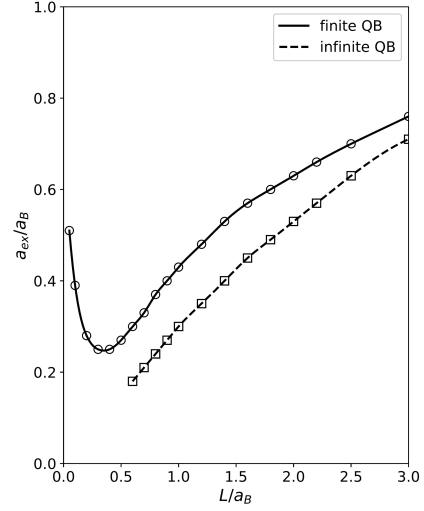


Fig. 3. Effective Bohr radius of the quantum confined exciton as a function of the quantum box size L . The exciton is confined in a quantum box with an infinite barrier (dashed line) and a finite $\text{Al}_{0.3}\text{Ga}_{0.7}\text{As}$ barrier (solid line).

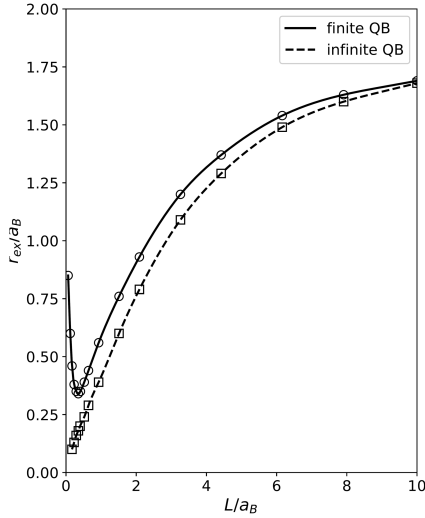


Fig. 2. Separation between the electron and the hole for the heavy-hole exciton as a function of the quantum box side L . The exciton is confined with an infinite barrier (dashed line) and a finite $\text{Al}_{0.3}\text{Ga}_{0.7}\text{As}$ barrier (solid line).

the same values of parameters as Koh et al. [16]. The GaAs parameters are $\varepsilon = 13.18$; $m_{e,w} = 0.0665m_0$; $m_{h,w} = 0.34m_0$ (for heavy-hole); $Ry = 4.35$ meV (effective Rydberg) and $a_B = 12.6$ nm (exciton Bohr radius). For the barrier, we have used $m_{e,b} = 0.09m_0$; $m_{h,b} = 0.466m_0$; $V_{0,e} = 243$ meV and $V_{0,h} = 140$ meV.

The binding energy of an exciton confined in a square box, with a finite and an infinite barrier, is shown in Fig. 1 as a function of the side box L . From this figure, we can see that for the infinite barrier,

the binding energy decreases with increasing box size. However, in the case of a finite barrier, the binding energy increases with increasing L , reaches a maximum value, and decreases monotonically. As L is increased, the binding energy approaches the value of the Rydberg unit. The peak in the binding energy occurs for the smallest values of L ($L \simeq 0.4$), where the probability of finding an electron or a hole outside the box is very weak. For a narrower quantum box (i.e., $L < 0.4$), the probability of finding an electron or a hole outside the box increases (weak confinement of the carriers), and this leads to a decrease in the binding energy. The effect of the confining potential becomes small when the box size increases ($L > 4a_B$). The present results are slightly superior to those found by Koh et al. [16] who considered a cylindrical form of the box.

In Fig. 2, we present the spatial extension of the exciton given by (19). For the infinite barrier case, this extension increases monotonically with increasing L . However, for the finite barrier case, r_{ex} decreases with lowering L , with a pronounced minimum near the value maximizing the binding energy, and increases again due to the delocalization of the wave function into the barrier layer. The electron-hole separation r_{ex} approaches the value of the bulk material (3D limit case) for large values of L .

The effective Bohr radius of the quantum-confined exciton a_{ex} is plotted in Fig. 3. It may be used for analysing the confinement effect and the quantum size effect on the exciton. Here, we find that a_{ex} decreases rapidly until it reaches a minimum and then increases as L decreases. A smaller exciton Bohr radius may be attributed to the localization of the exciton wave function. Therefore, as shown in Figs. 1 and 2, the smaller is the effective

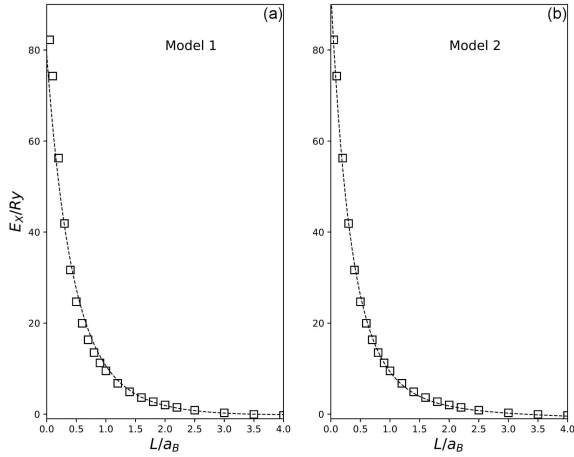


Fig. 4. Plot of the exciton energy versus L . The exciton is confined in a GaAs quantum box with a finite $\text{Al}_{0.3}\text{Ga}_{0.7}\text{As}$ barrier. Squares are calculated values. The dashed line is (a) the plot of the model 1, $E_X = 80 \exp(0.27L^2 - 2.2L) - 1$, and (b) the plot of the model 2, $E_X = 94 \exp(-0.07L^3 + 0.66L^2 - 2.8L) - 1$.

Bohr radius of the exciton, the greater is the binding energy and the smaller is the electron-hole separation r_{ex} .

In Fig. 4, we present the exciton energy E_X versus L . The exciton is confined in a GaAs quantum box with a finite $\text{Al}_{0.3}\text{Ga}_{0.7}\text{As}$ barrier. Squares are values calculated using (7), i.e., $E_X = E_e + E_h - E_b$. The optical gap is $E = E_X + E_g$, where E_g is the GaAs energy gap ($E_g = 1.424$ eV). It should be noted that the confinement energies of electrons are two to four times higher than those of holes as a result of the huge effective mass of heavy-holes compared to that of electrons. Figure 4 shows that the exciton energy increases monotonically with decreasing L . So, compared to a bulk semiconductor, the optical gap is very influenced by confinement in a quantum box and varies more strongly when $L < a_B$. This allows the adjustment of the optical gap of nanostructures across their sizes.

The empirical laws of energy variation of an exciton confined in a 0D nanostructure have been reported as a function of its dimension L . Yu et al. [26] proposed the law $E_X = A/L^B$. On the other hand, Wu et al. [1] proposed the law $E_X = A/\exp(L^B)$. In these two expressions, A and B designate adjustment parameters, where $B < 2$ in the first and $0 < B < 1$ in the second. Here, we revisit this dependence and propose two empirical models. The first model is shown as a dashed line in Fig. 4a, where we take $E_X = 80 \exp(0.27L^2 - 2.2L) - 1$. The second model, shown in Fig. 4b as the dashed line, is plotted with the expression $E_X = 94 \exp(-0.07L^3 + 0.66L^2 - 2.8L) - 1$. The second law agrees very well with the calculated exciton energy values, and make it possible to find the 3D limit of the bulk semiconductor $E_X = -Ry$.

4. Conclusion

In conclusion, using a variational calculation using the two band model and the effective mass approximation, we established a set of analytical equations to be used for calculating the properties of the excitons confined in a quantum box with a rectangular potential profile. We have tested the validity of the equations by checking the properties of the exciton in a bulk semiconductor (3D) and confined in a plane (2D). The calculations are clearly simplified in the case of confinement with an infinite barrier. Finally, we note that the perspective of application of the model developed in this paper remains widely open. Owing to its simplicity, it can be extended without difficulty to many types of applications, such as exploring new potential profiles of the quantum box, investigating higher excited states of the exciton, and calculating transitions energy and oscillator strengths for these states, examining electric and magnetic field effects, etc. However, it should be noted that the application of the model requires knowledge of the solution of the one-particle problem. Nevertheless, the work involved in obtaining the binding energy and other properties of the exciton is considerably reduced using analytical equations, making it easy to apply to any potential profile.

References

- [1] S. Wu, L. Cheng, Q. Wang, *Mater. Res. Express* **4**, 085017 (2017).
- [2] G. Wei, S. Wang, G. Yi, *Microelectron. J.* **39**, 786 (2008).
- [3] Y. Kubota, K. Nobusada, *Phys. Lett. A* **369**, 128 (2007).
- [4] S. Das, S. Dhar, *Superlattices Microstruct.* **103**, 145 (2017).
- [5] J.L. Marin, R. Riera, S.A. Cruz, *J. Phys. Condens. Matter* **10**, 1349 (1998).
- [6] P. Sujana, A. John Peter, C.W. Lee, *Physica E* **72**, 63 (2015).
- [7] M. Revathi, C.K. Yoo, A. John Peter, *Physica E* **43**, 322 (2010).
- [8] W. Xie, *Physica B* **304**, 112 (2001).
- [9] R.A. Escorcía, R. Robayo I.D. Mikhailov, *Phys. Status Solidi (b)* **230**, 431 (2002).
- [10] S. Tilouche, A. Sayari, M. Omri, S. Souilem, L. Sfaxi, R. M'Ghathi, *Mater. Sci. Semicond. Process.* **124**, 105614 (2021).
- [11] O. Mommadi, A. El Moussaouy, M. Chnafi, M. El Hadi, A. Nougouy, H. Magrez, *Physica E: Low-dimen. Syst. Nanostruct.* **118**, 113903 (2020).
- [12] N.S. Minimala, A. John Peter, C.W. Lee, *Physica E* **48**, 133 (2013).

- [13] X. Zhao, S.-Y. Wei, C.-X. Xia, *Physica E* **43**, 1076 (2011).
- [14] S.A. Safwan, M.H. Hekmat, A.S. Asmaa, *Physica E* **41**, 150 (2008).
- [15] Z. Barticevic, M. Pacheco, C.A. Duque, L.E. Oliveira, *Phys. Rev. B* **68**, 073312 (2003).
- [16] T.S. Koh, Y.P. Feng, X. Xu, H.N. Spector, *J. Phys. Condens. Matter* **13**, 1485 (2001).
- [17] C Heyn, A. Radu, J.A. Vinasco et al., *Opt. Laser Technol.* **139**, 106953 (2021).
- [18] A. Tiutiunnyk, V. Akimov, V. Tulupenko, M.E. Mora-Ramos, E. Kasapoglu, F. Ungan, I. Sökmen, A.L. Morales, C.A. Duque, *Physica B: Condensed Matter* **484**, 95 (2016).
- [19] C. Cornet, J. Even, S. Loualiche, *Phys. Lett. A* **344**, 457 (2005).
- [20] P. Harrison, *Quantum Wells, Wires and Dots*, 2nd ed., Wiley, London 2005.
- [21] H. Gotoh, H. Ando, *J. Appl. Phys.* **82**, 1667 (1997).
- [22] J. Planelles, J.I. Climente, *Comput. Phys. Commun.* **261**, 107782 (2021).
- [23] J. Diouri, A. Taqi, A. El Haddad, M. Katih, E. Feddi, *Semicond. Sci. Technol.* **18**, 377 (2003).
- [24] P. Harrison, T. Piorek, W.E. Hagsto, T. Stirner, *Superlattices Microstruct.* **20**, 45 (1996).
- [25] G.W. Bryant, *Phys. Rev. B* **37**, 8763 (1988).
- [26] H. Yu, J. Li, R.A. Loomis, L.W. Wang, W.E. Buhro, *Nat. Mater.* **2**, 517 (2003).